Real-time prediction of the week-ahead flood index using hybrid deep learning algorithms with synoptic climate mode indices

A. A. Masrur Ahmed[a, b,*], Shahida Farheen[c], Thong Nguyen-Huy[d, e, f], Nawin Raj[a], S Janifer Jabin Jui[a], S. Z. Farzana[c]

[a]School of Mathematics, Physics, and Computing, University of Southern Queensland, Springfield, QLD, 4300, Australia; masrur@outlook.com.au (AAMA); nawin.raj@usq.edu.au (N. Raj), sjanifer.jui@usq.edu.au (SJJJ)

[b]Department of Infrastructure Engineering, University of Melbourne, Parkville, VIC 3010, Australia; abulmasrur.ahmed@unimelb.edu.au

[c]Department of Civil Engineering, Leading University, Sylhet-3112, Bangladesh. mailto:shahidafarheen196@gmail.com (S Farheen); zehan_farzana@lus.ac.bd (S. Z. Farzana)

[d]SQNNSW Drought Resilience Adoption and Innovation Hub, University of Southern Queensland, Toowoomba, QLD 4350, Australia; thong.nguyen-huy@usq.edu.au

[e]Centre for Applied Climate Sciences, University of Southern Queensland, Toowoomba, QLD 4350, Australia

[f]Ho Chi Minh City Space Technology Application Center, Vietnam National Space Center, VAST, Ho Chi Minh, Vietnam

Corresponding Author*: A. A. Masrur Ahmed (abulmasrur.ahmed@unimelb.edu.aumailto:)

Abstract

This paper aims to propose a hybrid deep learning (DL) model that combines a convolutional neural network (CNN) with a bi-directional long-short term memory (BiLSTM) for week-ahead prediction of daily flood index (I_F) for Bangladesh. The neighbourhood component analysis (NCA) is assigned for significant feature selection with synoptic-scale climatic indicators. The results successfully reveal that the hybrid CNN-BiLSTM model outperforms the respective benchmark models based on forecasting capability, as supported by a minimal mean absolute error and high-efficiency metrics. With respect to I_F prediction, the hybrid CNN-BiLSTM model shows over 98% of the prediction errors were less than 0.015, resulting in a low relative error and superiority performance against the benchmark models in this study. The adaptability and potential utility of the suggested model may be helpful in subsequent flood monitoring and may also be beneficial to policymakers at the federal and state levels.

Keywords flood index, climate indices, deep hybrid learning; feature extraction, Bangladesh

Nomenclature

ABMR	All Bangladesh Monsoon Rainfall
ACF	Autocorrelation Function
ANN	Artificial Neural Network
AO	Arctic Oscillation
AWRI	Available Water Resources Index
BiLSTM	Bi-directional Long- short term memory
BMD	Bangladesh Meteorological Department
BOB	Bay of Bengal

BOM	Australian Bureau of Meteorology
BWDB	Bangladesh Water Development Board
CNN-BiLSTM	Hybrid Model integrating the CNN with BiLSTM
CCF	Cross Correction Function
CNN	Convolutional Neural Network
DL	Deep Learning
DMI	Dipole Model Index
EMI	El-Nino southern oscillation Modoki index
ENSO	El Niño Southern Oscillation
EPI	East Pole Index
E_P	Effective Precipitation
FC	Fully Connected
GBI	Greenland Block Index
GRU	Gated Recurrent Unit
I_F	Flood Index
IOD	Indian Ocean Dipole
IPO	Interdecadal Pacific Oscillation
KNMI	Royal Netherlands Meteorological Institute
LM	Legates-McCabe's Index
LSTM	Long- short term memory
MAE	Mean Absolute Error
MAPE	Mean Absolute Percentage Error
MSE	Mean Squared Error
NAO	North Atlantic Oscillation
NCA	Neighbourhood Component Analysis

NOAA	National Oceanic and Atmospheric Administration
NSE	Nash–Sutcliffe Efficiency
NSW	New South Wales
PACF	Partial Autocorrelation Function
PDO	Pacific Decadal Oscillation
QGIS	Quantum GIS
r	Correlation Coefficient
RAM	Random Access Memory
ReLU	Rectified Linear Unit
RMSE	Root-Mean-Square-Error
SAM	Southern Annular Mode
SGD	Stochastic Gradient Descent Optimization
SOI	Southern Oscillation Index
SST	Sea Surface Temperature
STR	Subtropical Ridge
SVR	Support Vector Regression
TPI	Tri-pole Index
WPI	West Pole Index

1 Introduction

Floods cause considerable damage in South Asia than in any part of the world (Matheswaran et al., 2018). The most affected areas are grasslands, mountain forest ecosystems of the Himalayas, and the Sundarbans (Hasnat et al., 2018). Bangladesh lies geographically at the confluence of three large rivers, the Ganges, Brahmaputra, and Meghna, with about 92.5% of the basin area outside its boundaries (Khairul et al., 2022). Most of the monsoon rainfall and

its water runoff flow through its river network, which might severely exceed the capacity of the drainage channels and cause flooding. Examples of major flood events are 1954, 1955, 1974, 1987, 1988, 1998, 2004, 2007, and 2012, which inundated from 20.5% up to 70% of the country on average (Alam et al., 2021). Therefore, it is essential to quantify the direct and indirect costs and hazards of floods to take primitive measures before the events, which requires predictive information of flood characteristics, for example, the start time (flood onset), duration, volume, and peak level.

Because of the high probability and massive impact of flood events, the success of seasonal forecasts and the warning system is critical in seasonal flood management in Bangladesh (Chowdhury, 2005). Accurate and timely prediction of floods can help the relevant stakeholders minimize their drastic effects. Furthermore, government policies can be drawn to identify various options for mitigation. For example, successful flood policies will strengthen relevant planning and implantation agencies (Brammer, 1990). Thus, there is tremendous potential for hydrologic models to be helpful in various applications, particularly in the context of flood preparedness and planning for future climate variability.

Many flood inundation models have been developed recently and effectively implemented in various parts (Bhagabati & Kawasaki, 2017). Despite such models can simulate detailed flood dynamics, they suffer from several significant shortcomings. The significant restrictions of flood inundation models consist of the requirement of complicated data inputs, computational effort, and differences in modelling results (Teng et al., 2017).

The flood index (I_F) is an alternative candidate for supporting disaster management and flood risk assessment in simplicity and practical applicability (Cian et al., 2018). The development of I_F often requires simple inputs such as streamflow or precipitation. The I_F has been demonstrated to be a reliable and effective mathematical tool for determining whether or

not a given area is flooded at a specific time and location (Quintero et al., 2020). The I_F has also been successfully implemented to monitor flood conditions and characteristics (Moishin et al., 2021b). The reliable and accurate prediction of I_F is critical for early warnings that different societies can use for better management and mitigation.

Prediction of I_F using artificial intelligence methods has developed rapidly in recent years. For example, Prasad et al. (2021) proposed an M5 tree-based machine learning (ML) model integrated with advanced multivariate empirical mode decomposition to predict daily I_F values in Lockyer Valley in southeast Queensland, Australia. Moishin et al. (2021a) developed a hybrid deep learning (DL) model, combining Convolutional Neural Network (CNN) and Long Short-Term Memory (LSTM) to predict the daily I_F in Fiji. The results indicated that the hybrid DL model outperformed the standalone model (LSTM) and machine learning model (Support Vector Regression). Technically, DL models employ many feature extraction layers to efficiently extract non-linear and complex compound connections from data (Ghimire et al., 2019). Additionally, DL algorithms are highly effective in extracting data attributes when handling enormous volumes of complicated data and possessing strong computational and sophisticated mapping capabilities (Gong et al., 2019).

Several studies have demonstrated the influence of large-scale climate indices on monsoon precipitation in the Indian subcontinent, however varying depending on the geographic variation of the region (Kumar et al., 1999; Roy & Tedeschi, 2016; Xavier et al., 2007). Han and Webster (2002) showed that the Indian Ocean Dipole (IOD) occurrences significantly influence sea-level changes in the Bay of Bengal and that sea level anomalies in the northern bay may be a predictor of flooding and cholera outbreaks in Bangladesh. Gill et al. (2015) studied correlations between seasonal rainfall and Pacific sea surface temperatures (SSTs) to reveal spatially distinct relationships between El Niño–Southern Oscillation (ENSO) and Indian summer monsoon rainfall over the entire monsoon season, as well as three sub

146 seasons. Furthermore, the interactions between large-scale climate indices, e.g., IOD and
147 ENSO can affect the relationship between individual climate indices (e.g., ENSO) and Indian
148 summer monsoon rainfall (Pothapakula et al., 2020). Because of the well-known complicated
149 relationship between the monsoon season and ENSO, the large-scale climate drivers likely have
150 a significant role in regulating the food potential of Bangladesh (Ghose et al., 2021; Islam et
151 al., 2021).

152 This research aims to examine how the extreme phases of climate indices affect the
153 week ahead I_F in the region of Bangladesh. We developed a novel hybrid DL model (i.e., CNN-
154 BiLSTM) by incorporating a Neighbourhood Component Analysis (NCA) algorithm to
155 optimise the significant predictors. The DL methods such as LSTM and gated recurrent
156 networks (GRU) have shown an effective predictive methodology in hydrology and water
157 resources (Ahmed, Deo, Feng, et al., 2021; Ahmed, Deo, Raj, et al., 2021). Moreover, the CNN
158 algorithm can extract relevant features of the predictor variables (Ghimire et al., 2019). In the
159 past researches (Ahmed, Deo, Feng, et al., 2021; Ghimire et al., 2019), incorporating CNN and
160 an LSTM or GRU model has shown significant performance in predicting hydrological
161 variables. Nonetheless, to our best knowledge, such incorporation has not been piloted in I_F
162 prediction yet, particularly in Bangladesh. Thus, this research addresses the gap in research that
163 needs to be taken for developing countries such as Bangladesh using advanced DL
164 methodology for extreme weather events.

165 **2 Theoretical overview of data intelligent models**

166 *2.1 Convolutional neural network (CNN)*

167 The Convolutional Neural Network (CNN) is proposed by LeCun et al. (1989). CNN reduces
168 parameters and overfitting risk by processing input data via local connections and parameter sharing
169 (Zang et al., 2020). CNN has been extensively used in image recognition, natural language

processing, and time series prediction (Ahmed, Deo, Feng, et al., 2021; Ahmed, Deo, Raj, et al., 2021; Cannizzaro et al., 2021).

A convolutional layer in CNN incorporates various convolution kernels for extracting different features. Convolutional and pooling layers combine to minimise parameters and accelerate computations (Ghimire et al., 2022). The fully connected layer then uses the convolution kernel's features to calculate the final prediction. Additionally, in the fully connected layer of the architecture, all of the parameters for logic inference are learned from training data (Ghimire et al., 2021). The mathematical notation of feature extraction by one-dimensional convolution is explained as:

$$a_j^{(l+1)}(\tau) = \sigma(b_j^l + \sum_{f=1}^{F^l} K_{jf}^l(\tau) * a_f^l(\tau)) = \sigma(b_j^l + \sum_{f=1}^{F^l} [\sum_{p=1}^{p^l} K_{jf}^l(p) a_f^l(\tau - p)]) \quad (1)$$

where $a_j^{(l+1)}(\tau)$ denotes feature map j in layer l, σ means non-linear function, F^l denotes number of feature maps in layer l, K_{jf}^l denotes the kernel convolved over feature map f in layer l to create the feature map j in layer $l+1$, p^l denotes the length of kernels in layer l and b_j^l denotes a bias vector. Figure 1 provides the basic architecture of CNN model.

2.2 Bi-directional long short term memory (BiLSTM)

The bidirectional long short-term memory (BiLSTM) is a long short-term memory architecture with LSTM layers in forward and backward directions (Peng et al., 2021). BiLSTM uses forwards and backward LSTM layers in its architecture, as seen in Figure 2(b). Each memory block has two LSTM layers. The created two hidden-layer states have opposing temporal sequences using the forward LSTM layer $S_t, t \in [1, T]$ and the backward LSTM layer $S_t', t \in [T, 1]$; These layer states are then combined to deliver the identical output (Ahmed et

al., 2022). The forwards and backwards LSTM layers, respectively, can learn about the past and future of the input sequence. (Wang et al., 2019).

The hidden layer state H_t of BiLSTM at time *t* contains forward $\overrightarrow{h_t}$ and backward $\overleftarrow{h_t}$:

$$\overrightarrow{h_t} = \overrightarrow{LSTM}\left(h_{t-1}, x_{t,} c_{t-1}\right), t \in [1, T] \quad (2)$$

$$\overleftarrow{h_t} = \overleftarrow{LSTM}\left(h_{t+1}, x_{t,} c_{t+1}\right), t \in [T, 1] \quad (3)$$

$$H_t = [\overrightarrow{h_t}, \overleftarrow{h_t}] \quad (4)$$

Here, *T* is the time series. The BiLSTM method has been successfully applied in hydrological prediction (Kang et al., 2020; Li et al., 2021; Prasad et al., 2018).

2.3 Support vector regression (SVR)

When dealing with limited sets of variables and pattern recognition with a high degree of dimension, Support Vector Regression (SVR) can solve problems. This technique depends on using a kernel function in a high-dimensional space. To calibrate the error between the kernel function and the target data, the relaxation and penalty coefficients are introduced. (Hamidi et al., 2015). For a particular training X, the input is first mapped onto a high-dimensional feature space ϕ(x) (kernel function). After that it follows similar structure of a linear model. The linear vector expression can be as follows:

$$f(x) = \omega \cdot \emptyset(x) + b \quad (5)$$

where the weight vector, the constant, the mapping function of non-linear transformationis ω , *b*, and ϕ(x) respectively. By reducing the model complexity, the constant *b* and coefficient ω are estimated by diminishing:

$$R_{reg}(f) = C\frac{1}{N}\sum_{i=1}^{N} L_{\varepsilon}(f(x_i), y_i) + \frac{1}{2}\|w\|^2 \quad (6)$$

$$L_{\varepsilon}(f(x) - y) = \begin{cases} |f(x) - y| - \varepsilon \ for |f(x) - y| \geq \varepsilon \\ 0 \qquad\qquad otherwise \end{cases} \quad (7)$$

213 Here, both the parameters C and ε are to be determined which influence the
214 generalization performance, and the loss function assesses estimation quality $L_\varepsilon(f(x_i), y_i)$,
215 known as ε intensive loss function. $C\frac{1}{N}\sum_{i=1}^{N} L_\varepsilon(f(x_i), y_i)$ is the empirical error and $\frac{1}{2}\|w\|^2$ is
216 the smoothness of the function. The trade-off between the experimental threat and the
217 smoothness of the model is denoted by C. Moreover, the dual problem, given as transfer the
218 optimization problem:

219 $$f(x) = \sum_{i=1}^{l}(\alpha_i - \alpha_i^*)k\,(x_i, x) + b \quad (8)$$

220 where, α_i and α_i^* are the introduced Lagrange multipliers and $k\,(x_i, x)$ is the kernel function.
221 The schematic structure of SVR is illustrated in Figure 2(a).

222 *2.4 Feature Selection: Neighbourhood Component Analysis (NCA)*

223 The feature selection plays a crucial role in developing predictive models. This is
224 because it enables a reduction in the number of input variables, thereby minimizing processing
225 costs, and improving the accuracy and interpretability of the model in terms of its properties
226 and predictors (Bowden et al., 2005; Maier et al., 2010; Prasad et al., 2018; Yang et al., 2012).
227 This study used Neighbourhood Component Analysis (NCA) to separate significant antecedent
228 lagged predictor variables from potential input variables. This method was developed by Yang
229 et al. (2012) and is non-rectilinear and non-parametric.

230 The NCA feature selection was performed using the *fsrnca* algorithm in MATLAB with
231 regularization, which was aimed at learning feature weights that minimize the average leave-
232 one-out regression loss across the training data. Through the NCA process, we trained a
233 variable set to obtain a better understanding of the characteristics by weighting and minimizing
234 the objective function while computing regression loss for soil moisture prediction.

235

In the fsrnca algorithm, a function $g(x)$: $\boldsymbol{R^P} \rightarrow \boldsymbol{R}$ is utilized to predict the response y based on several input variables, optimizing their nearest spaces. The weighted distance (D_w) between any two samples in the training set $T = \{(x_i, y_i): i = 1, 2, 3, \ldots, N\}$, where $x_i \in \boldsymbol{R^P}$ is the feature vectors (i.e., predictor variables) and $y_i \in \boldsymbol{R}$ is the target (i.e., the response variable), is calculated as follows:

$$D_w(x_a, x_b) = \sum_{j=1}^{J} w_j^2 \, |x_a, x_b| \quad (9)$$

During training, the *fsrnca* algorithm calculates the weighted distance (D_w) between two samples, x_a and x_b, by considering the weight, wj, associated with the jth feature. To improve the accuracy of the leave-one-out prediction during training, a probability distribution, $p_{\alpha\beta}$, is used. This probability represents the likelihood that x_α selects x_β as its reference argument. To select the feature subset and avoid overfitting, the algorithm uses a weighting vector, 'w', in conjunction with the gradient ascent method. A regularization component is included in this process to ensure that the model does not overfit the data.

3 Case study description and data

3.1 Study locations

In this study, we validated 34 stations in Bangladesh (Figure 3(a), Table A1) to predict the I_F using a hybrid DL model (i.e., CNN-BiLSTM). Bangladesh is a riverine country situated in the Ganges Delta, having a sub-tropical monsoon climate. Bangladesh lies in a unique position (20°45'N to 26°40'N and from 88°05'E to 90°45'E) where northern Bangladesh is in the foothills of the Himalayas, located in the Meghalaya Plateau, the Assam hill in the East, the Gangetic plain in the West and the Bay of Bengal in the South (Ahmed & Kim, 2003). The average annual rainfall varies between 2100 to 5100 mm, and 80% occurs during the monsoon (June to October) (BWDB, 2019). Bangladesh has 80% of the land in the floodplain areas, and over 50% is within 5m above sea level (Chowdhury, 1998; Rahman, 2010). Due to heavy

rainfall and eventual flooding, the country suffers enormous impacts on its agriculture, economy, infrastructure, and population (Tingsanchali & Karim, 2005).

3.2 Flood Index (I_F)

The daily rainfall (mm) of 34 weather stations in Bangladesh was acquired from the Bangladesh Meteorological Department's Climate Division. In this study, the flood index (I_F), as the response variable of our proposed DL model, is estimated from the effective precipitation (E_P) followed by the principle in a recently published relevant study (Lu, 2009). Suppose E_m was the rainfall reported on any day, where m is between 1 to 365 and the summation length of the preceding day is N, E_P for that (current i^{th}) day over a duration D was:

$$E_{P_i} = \sum_{N=1}^{D} \left[\frac{\sum_{m=1}^{N} E_m}{N}\right] \tag{10}$$

In order to calculate the total amount of recent and accumulated precipitation, daily water loss (due to runoff, evapotranspiration, infiltration, etc.) and the length of accumulation , the Available Water Resources Index (*AWRI*) (Byun & Lee, 2002) is expressed as a function of weighting factor W summed over that duration:

$$AWRI = \frac{E_p}{W} \tag{11}$$

$$W = \sum_{N=1}^{N=D} \frac{1}{N} \tag{12}$$

In this study, we used the duration of 365 (D) days (ignoring the leap year for simplicity) as for the usual hydrological cycle and hence Equation (11) can be written as:

$$AWRI = E_1 + \frac{(W-1)E_2}{W} + \frac{(W-1-\frac{1}{2})E_3}{W} + \cdots + \frac{W-1-\frac{1}{2}-\cdots-\frac{1}{364})E_{365}}{W} \tag{13}$$

$$\approx E_1 + 0.85E_2 + 0.77E_3 + \cdots + 4.23 * 10^{-4}E_{365}$$

In order to account for the gradual depletion of available water supplies, equation (13) incorporates the E_P into an exponential time-dependent reduction function. That means the current day accounts for 100% of precipitation received 1 day before, ≈ 85% of that received 2 days before, ≈ 77% of that received 3 days before, and so on to ≈ 0.0423% of that received 365 days before. This is consistent with the physical rationale for diminishing water supply, as in rainfall-runoff models and latest studies of flood detection using daily data (Lu, 2009). However, this Equation is much simpler than rainfall-runoff models as it is useful for detecting whether there is an excess or shortage of water supplies that could lead to a flood catastrophe. This empirical model employs simply precipitation data and doesn't need any parameter estimates, unlike rainfall-runoff models, which have more complex data input specifications (Deo et al., 2018).

Reduced weight means the depletion of water supplies due to hydrological cycles. A few days after a rainstorm event, the loss in water resources is anticipated to reach its peak (Moishin et al., 2021b). This perspective assumes that recent downpours have a substantial impact on the risk of a flood. However, the proposed approach considers the accumulated impacts of previous rainfall fairly. Generaly, if the AWRI exceeds the average, the water supplies are relatively ample, indicating the risk of flooding (Han & Byun, 2006). As such, the Flood Index (I_F), a standardized metric, is expressed by equation (14):

$$I_F = \frac{ARWI - {}^{1983}_{2020}\overline{ARWI^{max}}}{\sigma\left({}^{1983}_{2020}\overline{ARWI^{max}}\right)} \tag{14}$$

where ${}^{1983}_{2020}\overline{ARWI^{max}}$ is the mean of annual maximum daily *AWRI* for the determined period 1983–2020 and $\sigma\left({}^{1983}_{2020}\overline{ARWI^{max}}\right)$ is the standard deviation. In light of this, the criterion of the daily I_F being more than zero can be used to determine the risk of flooding on any given day.

The severity of a flood event can be evaluated based on the sum of positive I_F values from the onset of the flood [t_{onset} i. e., the first day when $I_F > 0$] to its end [t_{end} , last day before $I_F < 0$]. The highest event of flood danger I_F^{max} is determined by identifying the maximum value of I_F from t_{onset} and t_{end}. The duration of the flood event, D_F, can be measured by calculating the number of days between t_{onset} and t_{end}. Notably, various characteristics of flood events can be measured and evaluated using a straightforward running-sum approach (Yevjevich, 1967):

$$I_F^{acc} = \sum_{t=t_{onset}}^{t=t_{end}} I_{F_t} \text{ t where } I_{F_t} > 1 \quad (15)$$

$$I_F^{max} = \max(I_F)_{t_{end}-t_{onset}} \quad (16)$$

$$D_F = t_{end} - t_{onset} \text{ (days)} \quad (17)$$

During a period of flooding, the index of the flood for a particular day *t* is denoted by I_{F_t}, and it is only relevant when $I_F > 0$ and $t_{onset} \leq t \leq t_{end}$. The regular I_F observed during the study period is a time-varying signal that generates positive or negative index values in response to significant (or low) rainfall, as established by Nosrati et al. (2010). A positive value of I_F indicates a flooding event, and the flood properties are analyzed during this period of flooding.

3.3 Large scale climate indices

Fifteen large-scale daily climate indices were utilised as predictor variables to anticipate the I_F using a hybrid DL CNN-BilSTM model. Table 1 provides the list of climate indices and respective sources. Figure 4 shows a map of the research area with oceanic representation used to determine the climatic mode indices.

3.4 Development of hybrid CNN-BiLSTM model

The proposed CNN-BiLSTM model was developed with a 3.6 GHz Intel i7 processor and 16 GB of RAM machine. The Python interface of the models uses *TensorFlow* (Abadi et al., 2016) and *Keras* (Ketkar, 2017) DL frameworks to generate a multi-phase CNN-BiLSTM model. Keras is a DL API that integrates with TensorFlow, a capable Python machine learning framework. Keras is a highly usable interface for modern DL techniques. Also, NCA is implemented in MATLAB R2020b. The predicted I_F is also visualised using *matplotlib* (Barrett et al., 2005) and *seaborn* (Waskom et al., 2020). Quantum GIS (QGIS) software was also utilised to visualise the study area and geographical plots. A list of nine statistical measures is employed to investigate the practical implications of forecasting models. The following stages were taken in the creation of the proposed CNN-BiLSTM model. The schematic workflows of the CNN-BiLSTM hybrid model are illustrated in Figure 1. The optimum architectures of the hybrid CNN-BiLSTM and BiLSTM-based predictive model are tabulated in Table 2.

3.4.1 Predictor variables selection

Despite the lack of a precise technique to determine whether model predictors are reliable (Tiwari & Adamowski, 2013), to select the time series of I_F 's lag-time memories and predictors for an appropriate framework, different techniques are applied. These methods include trial and error, autocorrelation function (ACF), partial autocorrelation function (PACF), and cross-correlation function (CCF) (Masrur Ahmed et al., 2021). A significant antecedent behaviour in terms of the lag of I_F from the predictors was found using the PACF (Tiwari & Adamowski, 2013; Tiwari & Chatterjee, 2011). By monitoring the statistical resemblance between the predictors and the dependent variable, the CCF is in charge of choosing the input signal pattern based on the antecedent lag of the predictors. For example, Figure 5 (a) depicts the r_{cross} between I_F and GBI and Niño1+2 at Sylhet and Khulna stations. According to the figure, previous monthly delays have been statistically significant. If we look at the climate indices, the GBI revealed significant r_{cross}, ranging from +0.60 to +0.68,

respectively. To increase the diversity, the correlation coefficient (r) between predictors (i.e., GBI and Niño1+2) and target (I_F) is illustrated in Figures 5(b) and 5(c). It is found that the earliest legs provided comparatively higher correlations.

The NCA method also tests the significant antecedent lag memories of large-scale climate indices and I_F. This method delivers the required improvements in prediction accuracy and understanding of its predictors' predictive model traits and nature while reducing the dimensionality of input variables and computing cost.

3.4.2 Hybrid CNN-BiLSTM model design

The proposed hybrid CNN-BiLSTM model is established by using a CNN as feature extraction and a BiLSTM as a predictive model. The primary task is the configuration of hyper-parameters and the optimisation of these parameters. A large number of hyper-parameters must be addressed to develop a successful DL method. For this experiment, the default *Keras* parameters are used for network initialisation. This is the set of default-training parameters: the number of epochs in the training set is 200; the batch size is five, and the look-up size is one. ReLU is applied to the CNN-BiLSTM and BiLSTM networks as an activation function (see Table 2).

In addition, the SGD optimiser is employed, with a learning rate of 0.001. The number of hidden layer units varies between 70 and 60 for all layers of DL models, depending on their architecture. A feature extraction method involving three convolution layers was used, with each layer having its own set of filter and kernel size parameters, such as (70, 4) and (60, 4), respectively. Mean Square Error (MSE) was used as a loss function in the model to represent the error. Aside from that, we scale the predictor variables between 0 and 1 using a min-max normalisation function. The missing values are filled in with the mean value of the same date.

The input data are divided into three sets to develop predictive models: training, testing, and validation. The model is trained on the same data set in each iteration. As a result, the model will better understand the data's features as it is trained. Validation sets are used to analyse and validate models during development as compared to training sets. The information obtained from this validation procedure is meant to be used to change the model hyperparameters as necessary. Finally, the testing phase is used only after a model has been trained (using the train and validation sets), and it is primarily used to evaluate the model. 39 years of data were used in this study, and 70% of the data sets were used for training, 15% for validation, and 15% for testing.

3.4.3 Performance metrics

The prediction performance was done by a rigorous and insightful evaluation of the objective model CNN-BiLSTM with other counterpart models. Our study evaluated multiple of graphical and statistical metrics in the independent testing phase. The paper uses statistical metrics such as Pearson's correlation coefficient (*r*), Mean Absolute Percentage Deviation (*MAPD*; %), Mean Absolute Error (*MAE*), Root Mean Squared Error (RMSE), and Nash–Sutcliffe Efficiency (*NSE*). The mathematical notations of the statistical parameters are listed below, Eq. (14-17).

$$\text{Mean Absolute Error } (MAE) = \frac{1}{n}\sum_{i=1}^{n}\left|I_F^{for} - I_F^{obs}\right| \tag{8}$$

$$\text{Nash} - \text{Sutcliffe Efficiency } (NSE) = 1 - \left[1 - \frac{\sum_{i=1}^{n}(I_F^{for})^2}{\sum_{i=1}^{n}\left(I_F^{obs} - \overline{I_F^{for}}\right)^2}\right] \tag{9}$$

$$\text{Correlation Coefficient } (r) = \left(\frac{\sum_{i=1}^{n}\left(I_F^{obs} - \overline{I_F^{obs}}\right)(I_F^{for} - \overline{I_F^{for}})}{\sqrt{\sum_{i=1}^{n}\left(I_F^{obs} - \overline{I_F^{obs}}\right)^2 \sum_{i=1}^{N}(I_F^{for} - \overline{I_F^{for}})^2}}\right)^2 \tag{10}$$

$$\text{Mean Absolute Percentage Error } (MAPD; \%) = \frac{1}{n}\left(\sum_{i=1}^{n}\left|\frac{(I_F^{for} - I_F^{obs})}{I_F^{obs}}\right|\right) * 100 \quad (11)$$

$$\text{Root Mean Square Error } (RMSE) = \sqrt{\frac{1}{n}\sum_{i=1}^{n}(I_F^{for} - I_F^{obs})^2} \quad (12)$$

$$\text{Percent Bias (PBIAS, \%)} = \frac{\sum_{i=1}^{n}\left|I_F^{for} - I_F^{obs}\right|}{\sum_{i=1}^{n}(I_F^{obs})} \quad (13)$$

Where I_F^{obs} is the the observed and I_F^{for} is the model-predicted value from the i^{th} element; $\overline{I_F^{obs}}$ and $\overline{I_F^{for}}$ show their average, respectively, and n denotes the number of observations of the I_F.

4 Results and discussions

4.1 Results of flood index prediction

We present a deep hybrid predictive model (CNN-BiLSTM) to predict the I_F of thirty-four selected stations in Bangladesh, compared with two benchmark models (i.e., BiLSTM and SVR). Statistical metrics and infographics were also used to understand the predictive capability of the proposed model. Overall, the proposed CNN-BiLSTM model was found to predict I_F values using large-scale climate indices accurately.

Figure 6 shows that, when compared to other benchmark models, the proposed hybrid DL model (CNN-BiLSTM) exhibits significant improvement in I_F prediction for a loop of thirty-four stations, as demonstrated by the evaluation metrices correlation coefficient (r) and mean absolute error (*MAE*). The figure also displays better distributions of r and *MAE* values of the CNN-BiLSTM model between the lower quartile (25th percentile) and the upper quartile (75th percentile) compared to BiLSTM and SVR, indicating the ability of accurate prediction of the proposed model for all the study sites. In addition, Table 3 shows that the proposed CNN-BiLSTM model yields better r-values ≈ 0.987 - 0.996, that it is superior to the BiLSTM model

414 with $r \approx 0.977$ - 0.993. On the other hand, the classical machine learning model (i.e., SVR) has
415 lower *r*-values ≈ 0.888 - 0.992. The same results were observed using the *MAE*. The proposed
416 hybrid DL prediction model outperforms the other two competing methods as demonstrated by
417 the *r* and *MAE* values.

418 Figure 7 contains further information on I_F prediction regarding the coefficient of
419 determination (R^2) and RMSE. In general, the newly developed CNN-BiLSTM model can
420 provide the highest value of R^2 and the lowest values of RMSE. The R^2 values generated by
421 the CNN-BiLSTM model ranged between 0.995 and 0.996 over 80% of the total stations. The
422 second candidate is the BiLSTM model, with R^2 ranging from 0.977 to 0.992, while the SVR
423 model has the lowest R^2 values of 0.965 to 0.991. Overall stations, the deep hybrid CNN-
424 BiLSTM prediction model outperformed other benchmark models.

425 Further evaluation of the predictive model (i.e., CNN-BiLSTM) is performed by scatter
426 plot, as shown in Figure 8. The scatter plot is plotted with the goodness-of-fit between predicted
427 and observed I_F and a least-square fitting line. As illustrated in Figure 8, the suggested model
428 outperforms the baseline model by a significant margin, with an R^2 value significantly higher
429 than the baseline model. The proposed hybrid DL model (CNN-BiLSTM) performed
430 noticeably better for the Sylhet station than for the other stations and models in terms of I_F
431 forecasting, recorded the magnitudes that were most similar to one (m|$R^2 \approx 0.656$|0.996),
432 followed by the BiLSTM (0.627|0.993) model. Additionally, the Comilla station exhibits
433 substantial performance with the proposed CNN-BiLSTM (0.65|0.997) model when compared
434 to the BiLSTM (0.64|0.994), and SVR (0.69|0.974) models, respectively. Hence, it is evident
435 that the DL hybrid CNN-BiLSTM predictive model is well appropriate for forecasting the
436 week-ahead I_F forecast.

A time series plot does further evaluation; the predictive abilities of the hybrid and standalone models that were used in the study are further established. Figure 9 compares the predicted and observed I_F time series plot between the proposed hybrid (i.e., CNN-BiLSTM) model and the standalone model (i.e., SVR). To illustrate, Figure 9 depicts the predicted I_F at two stations using the proposed model and classical machine learning model (i.e., SVR), resulting in an extremely near I_F to the one that was seen, showing that the model is highly predictable. A significant improvement in forecasted I_F was achieved due to the application of the NCA algorithm.

The inclusion of the Taylor diagram (Taylor, 2001) in the study adds additional support a more thorough analysis that proves how closely the correlation coefficients (r) are related to the predicted and observed I_F. The hybrid CNN-BiLSTM model in four selected stations with a pool of synoptic climate indices produces substantially similar output to the observed value than any other applied models. When it came to achieving the closest possible match to the observed data, the proposed model (i.e., CNN-BiLSTM) for the Rangpur and Sylhet stations is the closest. Regardless of improved performance, Ambagan and Chittagong stations showed much deviation from the observed I_F.

The promoting percentage of root means squared error (RMSE), Mean Absolute Error (MAE), and Mean Absolute Percentage Deviation (MAPD) are additional metrics used to evaluate the proposed deep hybrid CNN-BiLSTM model's predictive performance. It should be noted that the BiLSTM and SVR models are compared using the promoting percentage given as the incremental performance (∇) of the objective model over rival techniques. In addition, as shown in Figure 11, the assessment of ∇_{MAE}, ∇_{MAPD}, and ∇_{RMSE} significantly improves the corresponding parameters as compared to the traditional BiLSTM and SVR model. For the case of ∇_{MAE}The improvement is 1.1 to 25% and 0 to 50% for BiLSTM and

SVR accordingly. Similarly, ∇_{MAPD} (%) and ∇_{RMSE} (%) displayed comparable performance ranging from 0 to 89% and 0 to 98% and 6.3 to 91.8%, and 0.2 to 101.3% for BiLSTM and SVR. This demonstrates that our proposed model was the most responsive forecasting.

4.2 Discussions

Several studies, including Maplecroft (2011) and the United Nations (2015), have identified Bangladesh to be highly susceptible to climate change. Geographically, it is particularly prone to the physical consequences of climate change, with these consequences exacerbating the already-existing sustainability challenges that this densely populated country is dealing with (Mahmud & Prowse, 2012). The harmful effects can be lessened by locating, creating, and validating innovative scientific methodologies that can be used for flood-risk warning and regular monitoring, as well as flood risk reduction and adaptation. In addition, operational flood monitoring and decision-making demand the creation of an index that monitors daily or weekly flood extents, allowing for a more precise assessment of short-term events. A daily flood monitoring index can be used to determine the beginning, length, and intensity of flood event(s) for shorter period like week or month or for longer period like year (Nosrati et al., 2010).

Thus, predicted flood episodes between July 2019 and February 2020 were recorded and quantified for study sites selected based on the diverse classification of I_F as shown in Table 4. In the case of moderate to extreme flood events, it has been observed that the flood began almost the same week, with the longest duration found for the Hatiya station (200 days). Following the application of the CNN-BiLSTM model to a flood situation, it has been discovered that higher flood scenarios provide perfect forecasting with bias error ranges ranging from 0.67% to 49%. Chuadanga station performed exceptionally poorly in forecasting results, with a high percentage of bias in the forecasting results (50%). At the same time, flood

warnings were issued for Ambagan, Chittagong, Kepurpara, and Hatiya, which lasted for more than 190 days (consecutive days when $I_F > 0$).

We have addressed essential aspects of flood events, such as flood dangers, flood severity, peak floods, flood duration, and total precipitation. We find that the flood severity and peak flood are precisely the same. Observations have shown that when the flood intensity is highest, the peak flood also appears to be at its highest point. The findings also showed that the I_F was useful for estimating the duration, seriousness, and intensity of flood scenarios as well as for classifying the seriousness of flood situations. It has resulted that the newly developed hybrid CNN-BiLSTM model is based on the flood index feature, which is an important concept to understand. Predicting floods is critical for better flood management and mitigation planning.

5.0 Conclusions and outlook

Deep learning algorithms were used in this paper to develop a new artificial intelligence methodology for daily flood index forecasting. They were trained on synoptic mode indices and reliable ground-truth observations from thirty-four stations in Bangladesh. Our novel method, the hybrid CNN-BiLSTM model combines Convolutional Neural Networks (CNN) with a Bi-directional Long Short-term Memory (BiLSTM) network. It has been demonstrated that the CNN-BiLSTM model can produce significant improvements in predictive performance and outperforms all the benchmark models like BiLSTM and SVR.

Upon thorough assessment of the suggested hybrid CNN-BiLSTM model, we have concluded that our method represents a promising approach for developing a predictive model for understanding flood scenarios in Bangladesh. The proposed hybrid CNN-BiLSTM model's superior performance is supported by its high NSE (0.986–0.997) and low MAPD (1.01–3.59) values.

Beyond these prediction issues, the suggested deep hybrid model can be applied to a variety of complicated or difficult prediction tasks, including, among other things, the forecasting of wind speed, energy costs, and tidal energy. Moreover, incorporating global climate models (GCM) to predict the flood index under global warming scenarios for better flood hazard management and mitigation.

Acknowledgements

The climate mode indices are acquired from different data sources such as the Bureau of Meteorology, Australia, and NCEP. The Bangladesh Meteorological Department, Bangladesh, obtained the rainfall data. The flood index was calculated using the Matlab code prescribed by Moishin et al. (2021b). The authors thank all the reviewers and the editor for their thoughtful suggestions and the review process.

Credit authorship contribution statement

A. A. Masrur Ahmed: Writing - original draft, conceptualization, methodology, software, editing, proofreading, model development, and application. **Shahida Farheen:** Data curation, Writing, editing, and co-authorship of the manuscript. **Thong Nguyen-Huy:** Writing, editing, and co-authorship of the manuscript. **Nawin Raj:** Writing, editing, and co-authorship of the manuscript. **S Janifer Jabin Jui:** Writing, proofreading, and co-authorship of the manuscript. **S. Z. Farzana:** Editing.

References:

Abadi, M., Barham, P., Chen, J., Chen, Z., Davis, A., Dean, J., Devin, M., Ghemawat, S., Irving, G., & Isard, M. (2016). Tensorflow: A system for large-scale machine learning. 12th {USENIX} Symposium on Operating Systems Design and Implementation ({OSDI} 16),

Ahmed, A., Deo, R. C., Feng, Q., Ghahramani, A., Raj, N., Yin, Z., & Yang, L. (2021). Hybrid deep learning method for a week-ahead evapotranspiration forecasting. *Stochastic Environmental Research and Risk Assessment*, 1-19.

Ahmed, A., Deo, R. C., Raj, N., Ghahramani, A., Feng, Q., Yin, Z., & Yang, L. (2021). Deep Learning Forecasts of Soil Moisture: Convolutional Neural Network and Gated Recurrent Unit Models Coupled with Satellite-Derived MODIS, Observations and Synoptic-Scale Climate Index Data. *Remote Sensing*, *13*(4), 554.

Ahmed, A. A. M., Deo, R. C., Ghahramani, A., Feng, Q., Raj, N., Yin, Z., & Yang, L. (2022). New double decomposition deep learning methods for river water level forecasting. *Sci Total Environ*, *831*, 154722. https://doi.org/https://doi.org/10.1016/j.scitotenv.2022.154722

Ahmed, R., & Kim, I.-K. (2003). Patterns of daily rainfall in Bangladesh during the summer monsoon season: case studies at three stations. *Physical Geography*, *24*(4), 295-318.

Alam, A., Ahmed, B., & Sammonds, P. (2021). Flash flood susceptibility assessment using the parameters of drainage basin morphometry in SE Bangladesh. *Quaternary International*, *575*, 295-307.

Barrett, P., Hunter, J., Miller, J. T., Hsu, J.-C., & Greenfield, P. (2005). matplotlib--A Portable Python Plotting Package. Astronomical data analysis software and systems XIV,

Bhagabati, S. S., & Kawasaki, A. (2017). Consideration of the rainfall-runoff-inundation (RRI) model for flood mapping in a deltaic area of Myanmar. *Hydrological Research Letters*, *11*(3), 155-160.

Bowden, G. J., Dandy, G. C., & Maier, H. R. (2005). Input determination for neural network models in water resources applications. Part 1—background and methodology. *Journal of Hydrology*, *301*(1-4), 75-92. https://doi.org/10.1016/j.jhydrol.2004.06.021

Brammer, H. (1990). Floods in Bangladesh: II. Flood mitigation and environmental aspects. *Geographical Journal*, 158-165.

BWDB. (2019). Summary Of Rainfall In Bangladesh For The Year 2017 & 2018. Surface Water Processing Branch *Bangladesh Water Development Board*. http://www.hydrology.bwdb.gov.bd/img_upload/ongoing_project/756.pdf

Byun, H.-R., & Lee, D.-K. (2002). Defining three rainy seasons and the hydrological summer monsoon in Korea using available water resources index. *Journal of the Meteorological Society of Japan. Ser. II*, *80*(1), 33-44.

Cannizzaro, D., Aliberti, A., Bottaccioli, L., Macii, E., Acquaviva, A., & Patti, E. (2021). Solar radiation forecasting based on convolutional neural network and ensemble learning. *Expert Systems with Applications*, *181*, 115167. https://doi.org/https://doi.org/10.1016/j.eswa.2021.115167

Chowdhury, J. (1998). Some hydraulic aspects of floods in Bangladesh and their implications in planning. *Ali, MA, Hoque, MM, Rahman, R., and Rashid, S*, 209-217.

Chowdhury, M. R. (2005). Consensus seasonal Flood Forecasts and Warning Response System (FFWRS): An alternate for nonstructural flood management in Bangladesh. *Environmental Management*, *35*(6), 716-725.

Cian, F., Marconcini, M., & Ceccato, P. (2018). Normalized Difference Flood Index for rapid flood mapping: Taking advantage of EO big data. *Remote Sensing of Environment*, *209*, 712-730.

Deo, R. C., Adamowski, J. F., Begum, K., Salcedo-Sanz, S., Kim, D.-W., Dayal, K. S., & Byun, H.-R. (2018). Quantifying flood events in Bangladesh with a daily-step flood monitoring index based on the concept of daily effective precipitation. *Theoretical and Applied Climatology*, *137*(1-2), 1201-1215. https://doi.org/ 10.1007/s00704-018-2657-4

Ghimire, S., Deo, R. C., Casillas-Pérez, D., & Salcedo-Sanz, S. (2022). Boosting solar radiation predictions with global climate models, observational predictors and hybrid deep-machine learning algorithms. *Applied Energy*, *316*. https://doi.org/https://doi.org/10.1016/j.apenergy.2022.119063

Ghimire, S., Deo, R. C., Raj, N., & Mi, J. (2019). Deep solar radiation forecasting with convolutional neural network and long short-term memory network algorithms. *Applied Energy*, *253*. https://doi.org/10.1016/j.apenergy.2019.113541

Ghimire, S., Yaseen, Z. M., Farooque, A. A., Deo, R. C., Zhang, J., & Tao, X. (2021). Streamflow prediction using an integrated methodology based on convolutional neural network and

long short-term memory networks. *Scientific reports*, *11*(1), 17497. https://doi.org/10.1038/s41598-021-96751-4

Ghose, B., Islam, A. R. M. T., Kamruzzaman, M., Moniruzzaman, M., & Hu, Z. (2021). Climate-induced rice yield anomalies linked to large-scale atmospheric circulation in Bangladesh using multi-statistical modeling. *Theoretical and Applied Climatology*, *144*(3), 1077-1099.

Gill, E. C., Rajagopalan, B., & Molnar, P. (2015). Subseasonal variations in spatial signatures of ENSO on the Indian summer monsoon from 1901 to 2009. *Journal of Geophysical Research: Atmospheres*, *120*(16), 8165-8185.

Gong, G., An, X., Mahato, N. K., Sun, S., Chen, S., & Wen, Y. (2019). Research on Short-Term Load Prediction Based on Seq2seq Model. *Energies*, *12*(16). https://doi.org/10.3390/en12163199

Hamidi, O., Poorolajal, J., Sadeghifar, M., Abbasi, H., Maryanaji, Z., Faridi, H. R., & Tapak, L. (2015). A comparative study of support vector machines and artificial neural networks for predicting precipitation in Iran. *Theoretical and Applied Climatology*, *119*(3-4), 723-731.

Han, S. U., & Byun, H. R. (2006). The existence and the climatological characteristics of the spring rainy period in Korea. *International Journal of Climatology: A Journal of the Royal Meteorological Society*, *26*(5), 637-654.

Han, W., & Webster, P. J. (2002). Forcing mechanisms of sea level interannual variability in the Bay of Bengal. *Journal of Physical Oceanography*, *32*(1), 216-239.

Hasnat, G. T., Kabir, M. A., & Hossain, M. A. (2018). Major environmental issues and problems of South Asia, particularly Bangladesh. *Handbook of environmental materials management*, 1-40.

Islam, A. R. M. T., Islam, H. T., Shahid, S., Khatun, M. K., Ali, M. M., Rahman, M. S., Ibrahim, S. M., & Almoajel, A. M. (2021). Spatiotemporal nexus between vegetation change and extreme climatic indices and their possible causes of change. *Journal of Environmental Management*, *289*, 112505.

Kang, H., Yang, S., Huang, J., & Oh, J. (2020). Time series prediction of wastewater flow rate by bidirectional LSTM deep learning. *International Journal of Control, Automation and Systems*, *18*(12), 3023-3030.

Ketkar, N. (2017). Introduction to keras. In *Deep learning with Python* (pp. 97-111). Springer.

Khairul, I. M., Rasmy, M., Ohara, M., & Takeuchi, K. (2022). Developing Flood Vulnerability Functions through Questionnaire Survey for Flood Risk Assessments in the Meghna Basin, Bangladesh. *Water*, *14*(3), 369.

Kumar, K. K., Rajagopalan, B., & Cane, M. A. (1999). On the weakening relationship between the Indian monsoon and ENSO. *Science*, *284*(5423), 2156-2159.

LeCun, Y., Boser, B., Denker, J. S., Henderson, D., Howard, R. E., Hubbard, W., & Jackel, L. D. (1989). Backpropagation applied to handwritten zip code recognition. *Neural Computation*, *1*(4), 541-551.

Li, F., Ma, G., Chen, S., & Huang, W. (2021). An Ensemble Modeling Approach to Forecast Daily Reservoir Inflow Using Bidirectional Long-and Short-Term Memory (Bi-LSTM), Variational Mode Decomposition (VMD), and Energy Entropy Method. *Water Resources Management*, *35*(9), 2941-2963.

Lu, E. (2009). Determining the start, duration, and strength of flood and drought with daily precipitation: Rationale. *Geophysical Research Letters*, *36*(12).

Mahmud, T., & Prowse, M. (2012). Corruption in cyclone preparedness and relief efforts in coastal Bangladesh: Lessons for climate adaptation? *Global Environmental Change*, *22*(4), 933-943.

Maier, H. R., Jain, A., Dandy, G. C., & Sudheer, K. P. (2010). Methods used for the development of neural networks for the prediction of water resource variables in river systems: Current status and future directions. *Environmental Modelling & Software*, *25*(8), 891-909. https://doi.org/10.1016/j.envsoft.2010.02.003

Maplecroft, V. (2011). Climate change vulnerability index. Climate change risk atlas 2011. In: United Kingdom: Verisk Maplecroft.

639 Masrur Ahmed, A. A., Deo, R. C., Feng, Q., Ghahramani, A., Raj, N., Yin, Z., & Yang, L. (2021). Deep
640 learning hybrid model with Boruta-Random forest optimiser algorithm for streamflow
641 forecasting with climate mode indices, rainfall, and periodicity. *Journal of Hydrology*, *599*.
642 https://doi.org/https://doi.org/10.1016/j.jhydrol.2021.126350
643 Matheswaran, K., Alahacoon, N., Pandey, R., & Amarnath, G. (2018). Flood risk assessment in South
644 Asia to prioritize flood index insurance applications in Bihar, India. *Geomatics, Natural*
645 *Hazards and Risk*.
646 Moishin, M., Deo, R. C., Prasad, R., Raj, N., & Abdulla, S. (2021a). Designing deep-based learning
647 flood forecast model with ConvLSTM hybrid algorithm. *IEEE Access*, *9*, 50982-50993.
648 Moishin, M., Deo, R. C., Prasad, R., Raj, N., & Abdulla, S. (2021b). Development of Flood Monitoring
649 Index for daily flood risk evaluation: case studies in Fiji. *Stochastic Environmental Research*
650 *and Risk Assessment*, *35*(7), 1387-1402.
651 Nosrati, K., Saravi, M. M., & Shahbazi, A. (2010). Investigation of flood event possibility over Iran
652 using Flood Index. In *Survival and Sustainability* (pp. 1355-1361). Springer.
653 Peng, T., Zhang, C., Zhou, J., & Nazir, M. S. (2021). An integrated framework of Bi-directional Long-
654 Short Term Memory (BiLSTM) based on sine cosine algorithm for hourly solar radiation
655 forecasting. *Energy*, *221*, 119887.
656 Pothapakula, P. K., Primo, C., Sørland, S., & Ahrens, B. (2020). The synergistic impact of ENSO and
657 IOD on Indian summer monsoon rainfall in observations and climate simulations–an
658 information theory perspective. *Earth System Dynamics*, *11*(4), 903-923.
659 Prasad, R., Charan, D., Joseph, L., Nguyen-Huy, T., Deo, R. C., & Singh, S. (2021). Daily flood forecasts
660 with intelligent data analytic models: multivariate empirical mode decomposition-based
661 modeling methods. In *Intelligent Data Analytics for Decision-Support Systems in Hazard*
662 *Mitigation* (pp. 359-381). Springer.
663 Prasad, R., Deo, R. C., Li, Y., & Maraseni, T. (2018). Ensemble committee-based data intelligent
664 approach for generating soil moisture forecasts with multivariate hydro-meteorological
665 predictors. *Soil and Tillage Research*, *181*, 63-81.
666 https://doi.org/https://doi.org/10.1016/j.still.2018.03.021
667 Quintero, F., Krajewski, W. F., & Rojas, M. (2020). A flood potential index for effective
668 communication of streamflow forecasts at ungauged communities. *Journal of*
669 *Hydrometeorology*, *21*(4), 807-814.
670 Rahman, M. H. (2010). Ultra Poor Households' Flood Coping Strategies towards Food Security in Two
671 Flood Prone Regions. *Dhaka: USAID*.
672 Roy, I., & Tedeschi, R. G. (2016). Influence of enso on regional indian summer monsoon
673 precipitation—local atmospheric influences or remote influence from pacific. *Atmosphere*,
674 *7*(2), 25.
675 Taylor, K. E. (2001). Summarizing multiple aspects of model performance in a single diagram. *Journal*
676 *of Geophysical Research: Atmospheres*, *106*(D7), 7183-7192.
677 Teng, J., Jakeman, A. J., Vaze, J., Croke, B. F., Dutta, D., & Kim, S. (2017). Flood inundation modelling:
678 A review of methods, recent advances and uncertainty analysis. *Environmental Modelling &*
679 *Software*, *90*, 201-216.
680 Tingsanchali, T., & Karim, M. F. (2005). Flood hazard and risk analysis in the southwest region of
681 Bangladesh. *Hydrological Processes: An International Journal*, *19*(10), 2055-2069.
682 Tiwari, M. K., & Adamowski, J. (2013). Urban water demand forecasting and uncertainty assessment
683 using ensemble wavelet-bootstrap-neural network models. *Water Resources Research*,
684 *49*(10), 6486-6507.
685 Tiwari, M. K., & Chatterjee, C. (2011). A new wavelet–bootstrap–ANN hybrid model for daily
686 discharge forecasting. *Journal of Hydroinformatics*, *13*(3), 500-519.
687 United-Nations. (2015). *International Stratety for Disaster Reduction. Secretariat Global Assessment*
688 *Report on Disaster Risk Reduction 2015: Making Development Sustainable: the Future of*
689 *Disaster Risk Management* (Vol. 4). UN.

690 Wang, S., Wang, X., Wang, S., & Wang, D. (2019). Bi-directional long short-term memory method
691 based on attention mechanism and rolling update for short-term load forecasting.
692 *International Journal of Electrical Power & Energy Systems*, *109*, 470-479.
693 Waskom, M., Botvinnik, O., Ostblom, J., Gelbart, M., Lukauskas, S., Hobson, P., Gemperline, D. C.,
694 Augspurger, T., Halchenko, Y., & Cole, J. B. (2020). mwaskom/seaborn: v0. 10.1 (April 2020).
695 *zenodo*.
696 Xavier, P. K., Marzin, C., & Goswami, B. N. (2007). An objective definition of the Indian summer
697 monsoon season and a new perspective on the ENSO–monsoon relationship. *Quarterly*
698 *Journal of the Royal Meteorological Society: A journal of the atmospheric sciences, applied*
699 *meteorology and physical oceanography*, *133*(624), 749-764.
700 Yang, W., Wang, K., & Zuo, W. (2012). Neighborhood Component Feature Selection for High-
701 Dimensional Data. *JCP*, *7*(1), 161-168.
702 Yevjevich, V. M. (1967). *Objective approach to definitions and investigations of continental*
703 *hydrologic droughts, An* Colorado State University. Libraries].
704 Zang, H., Liu, L., Sun, L., Cheng, L., Wei, Z., & Sun, G. (2020). Short-term global horizontal irradiance
705 forecasting based on a hybrid CNN-LSTM model with spatiotemporal correlations.
706 *Renewable energy*, *160*, 26-41.
707 https://doi.org/https://doi.org/10.1016/j.renene.2020.05.150

708

Figures

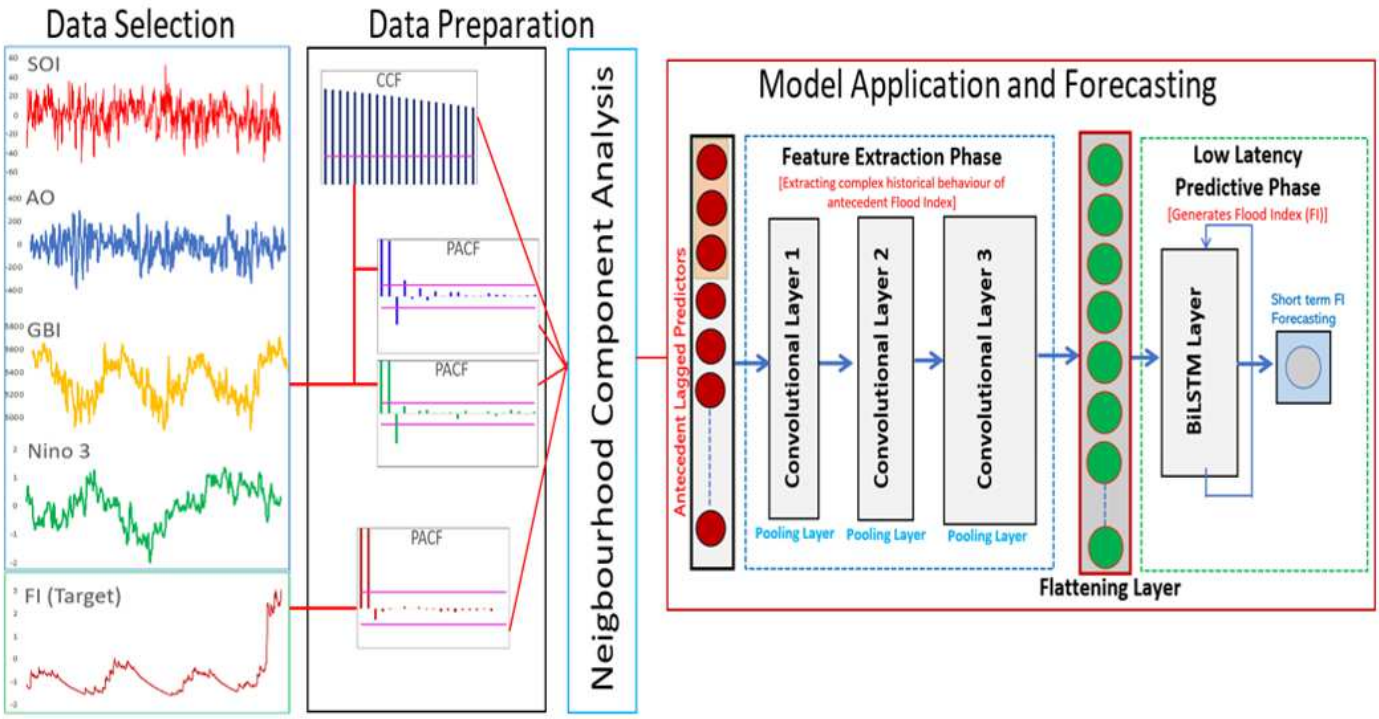

Figure 1

Schematic workflows of the CNN-BiLSTM hybrid model integrating neighborhood component analysis (NCA). The Hybrid CNN-BiLSTM integrates convolution neural network (CNN) and bi-directional long short-term memories (BiLSTM).

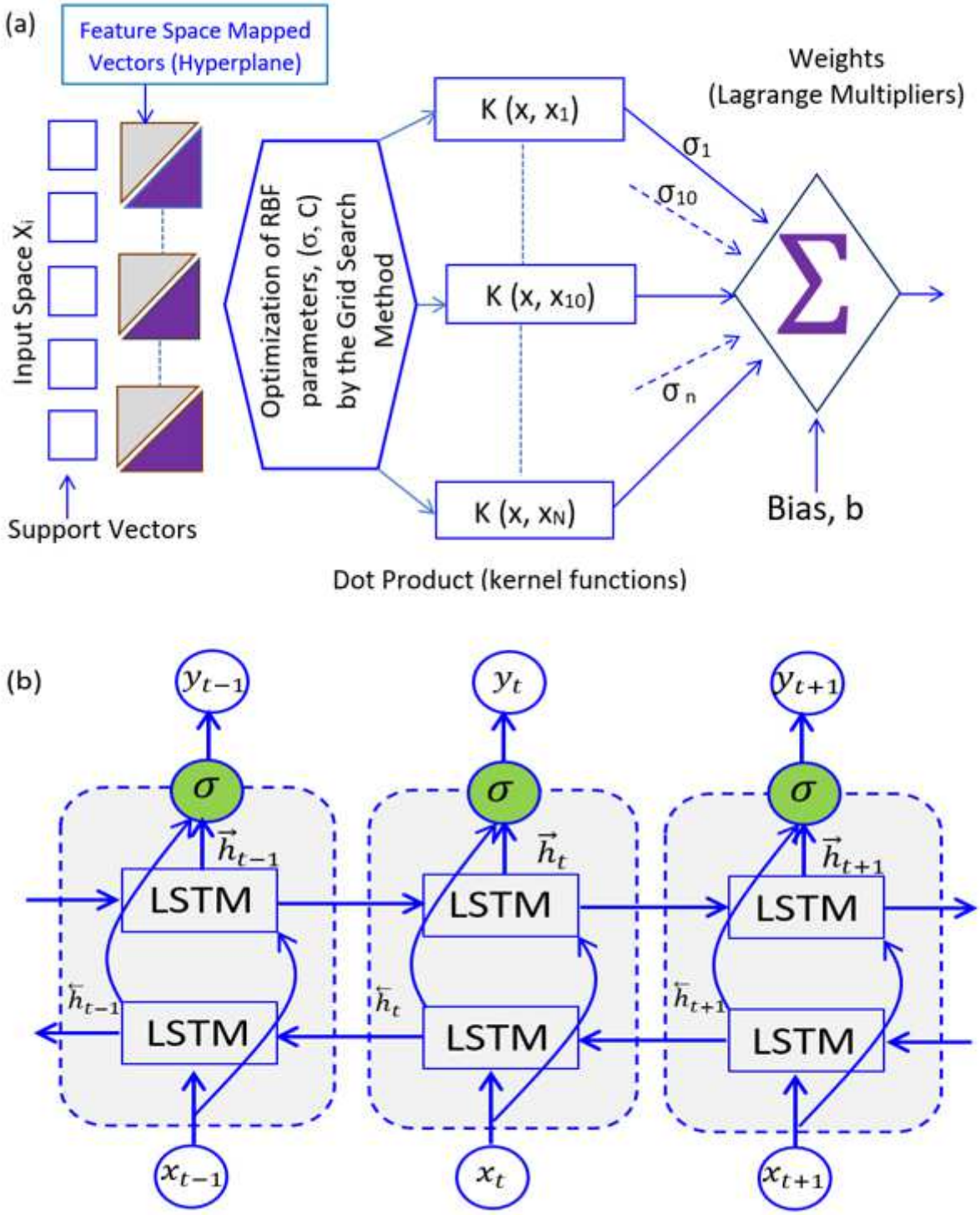

Figure 2

(a) Schematic structure of support vector regressions (SVR) and (b) Schematic structure of bidirectional LSTM (BiLSTM)

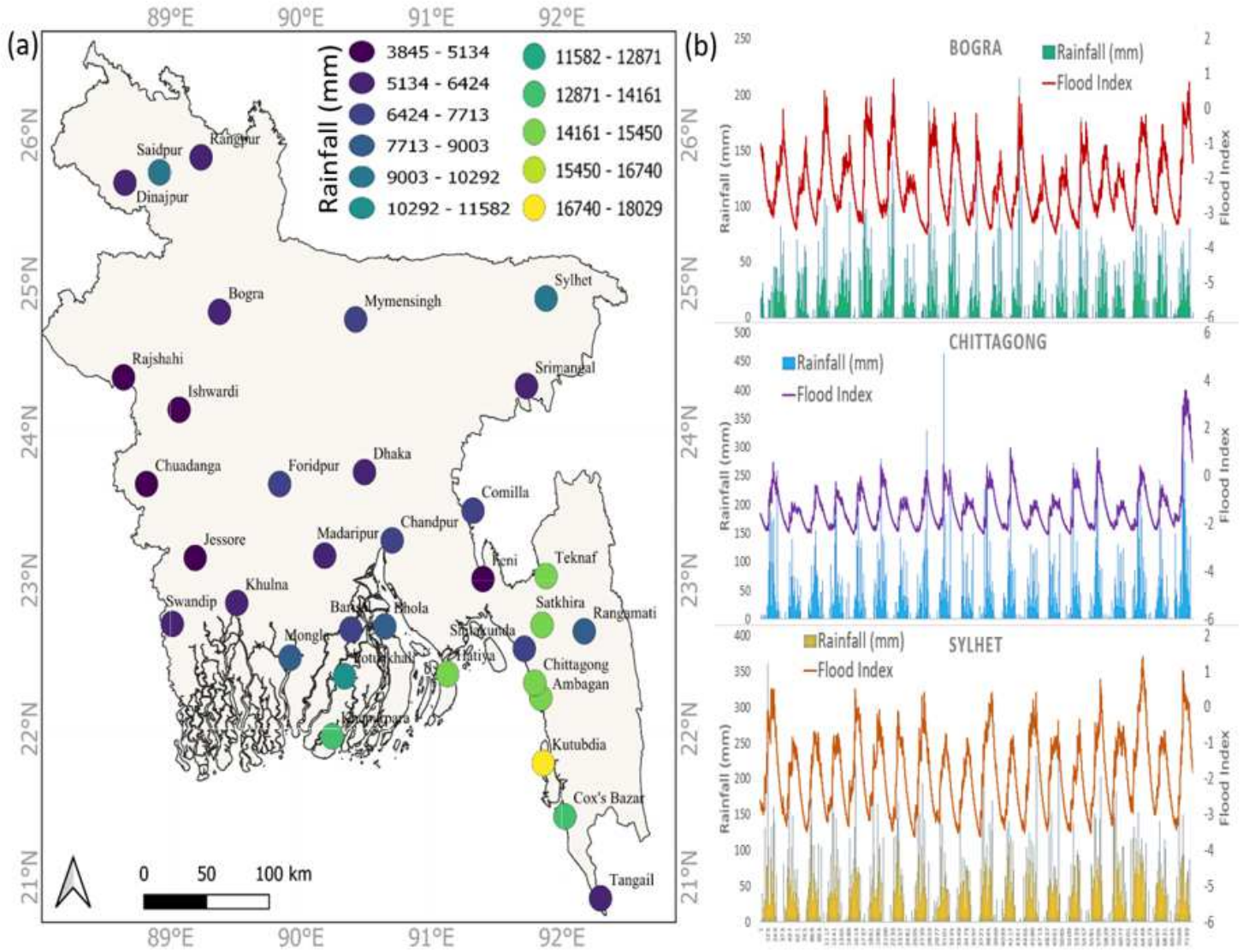

Figure 3

(a) The selected weather stations of Bangladesh with total rainfall of 2019, (b) Time series plot of rainfall (mm) vs. the flood index (I_F) of three selected stations (*i.e.,* Bogra, Chittagong, and Sylhet). Note: the list of geographical locations of the stations is tabulated in Table 1.

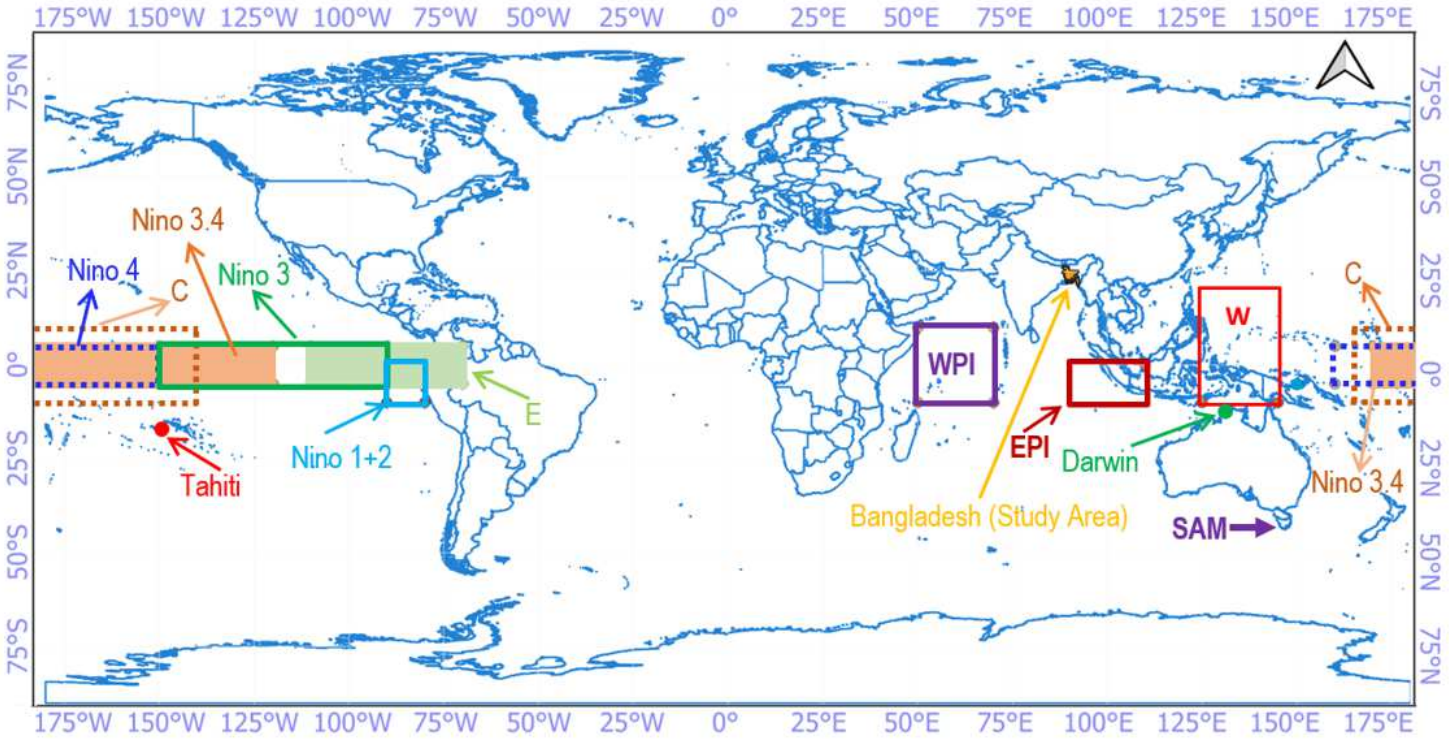

Figure 4

Map of the study region with oceanic representation used to calculate the climate mode indices (CI). The details of the climate mode indices are provided in Table 2.

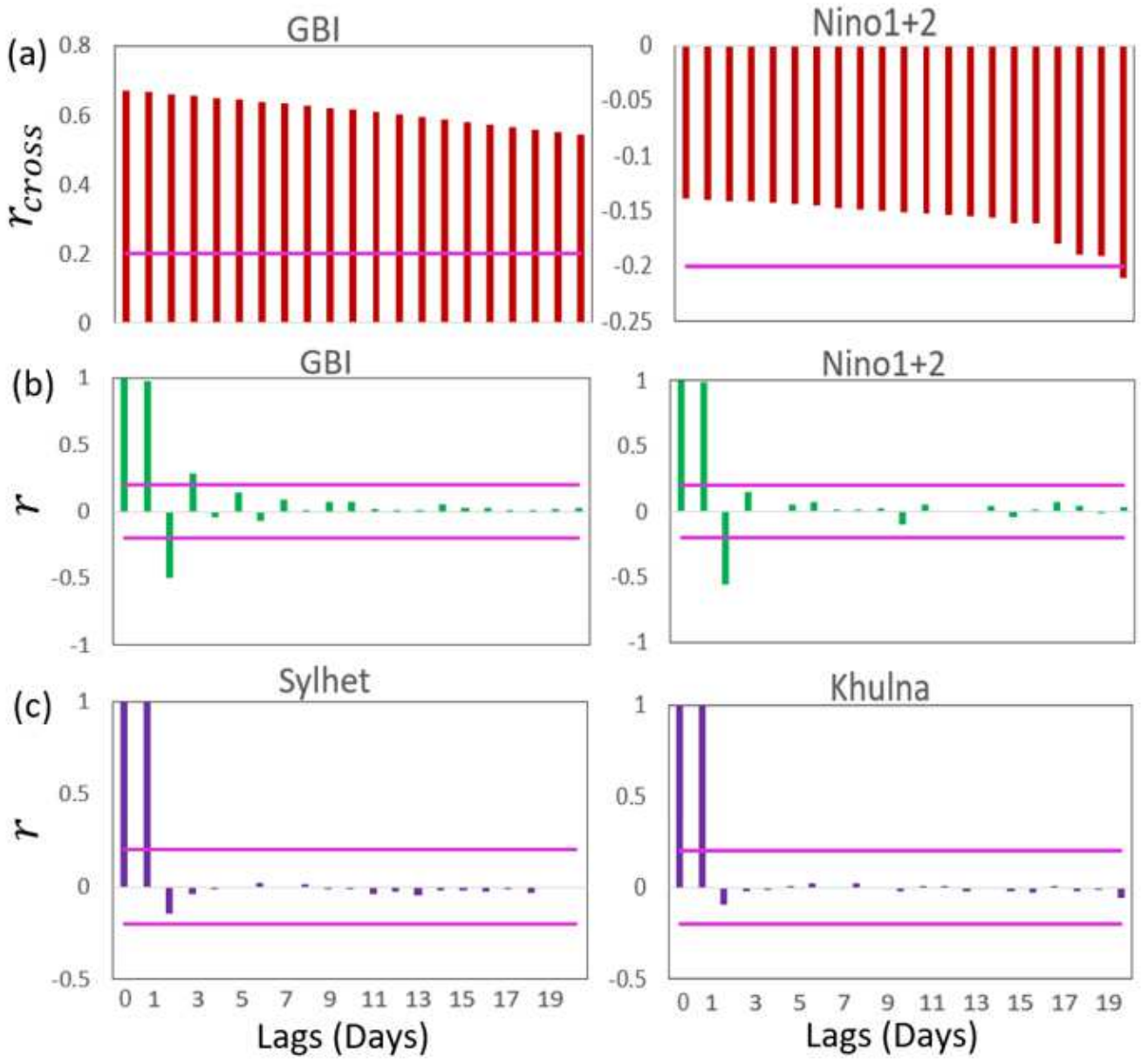

Figure 5

(a) Cross-correlation functions (CCF) showing the covariance between the objective variable (I_F) and the predictor variables (i.e., GBI and Nino1+2) for Sylhet stations, (b) Partial autocorrelation function (PACF) plot of the predictor variables (i.e., GBI and Nino 1+2) of Sylhet stations and (c) Partial autocorrelation function (PACF) plot of the target variable (i.e., I_F) of Sylhet and Khulna stations. The pink line in the figures indicates the ±95% confidence level.

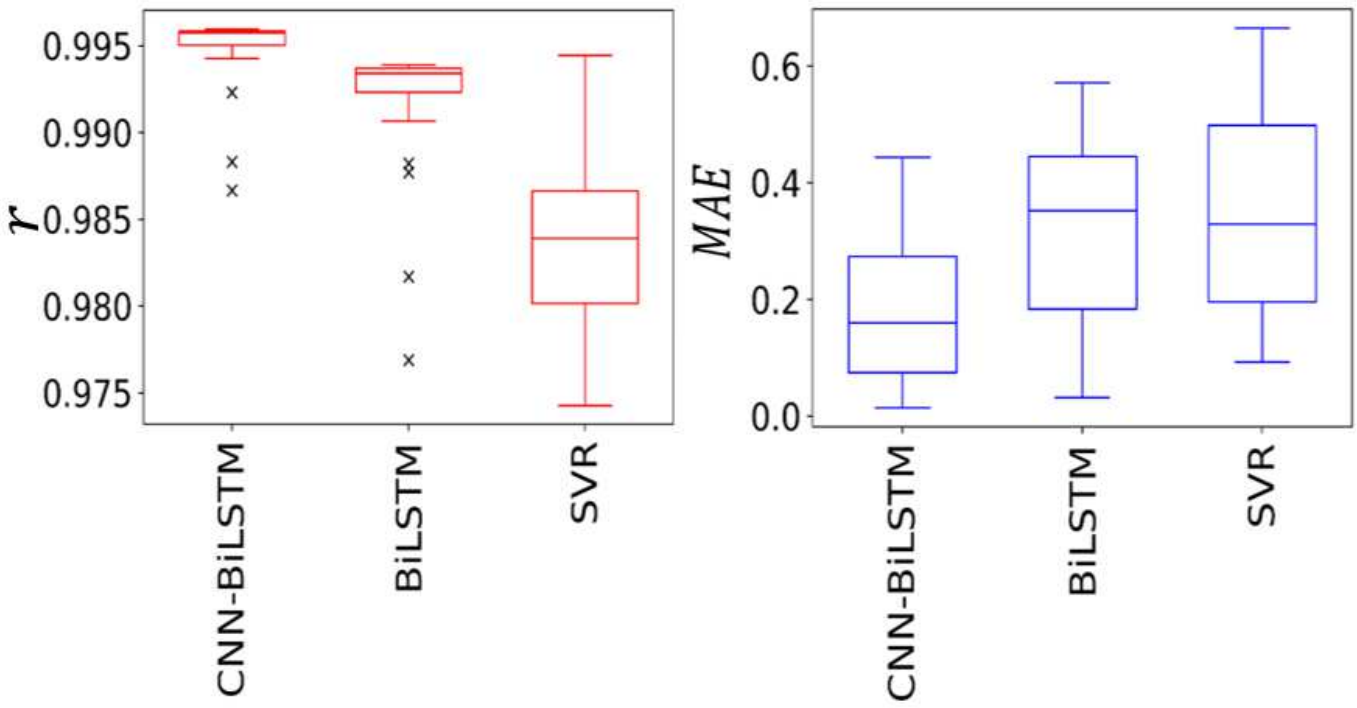

Figure 6

Box plots of proposed hybrid models (i.e., CNN-BiLSTM) compared with their respective standalone counterparts (i.e., BiLSTM and SVR) in predicting I_F in terms of Correlation Coefficient (r) and Mean Absolute Error (MAE) for 34 selected stations in Bangladesh.

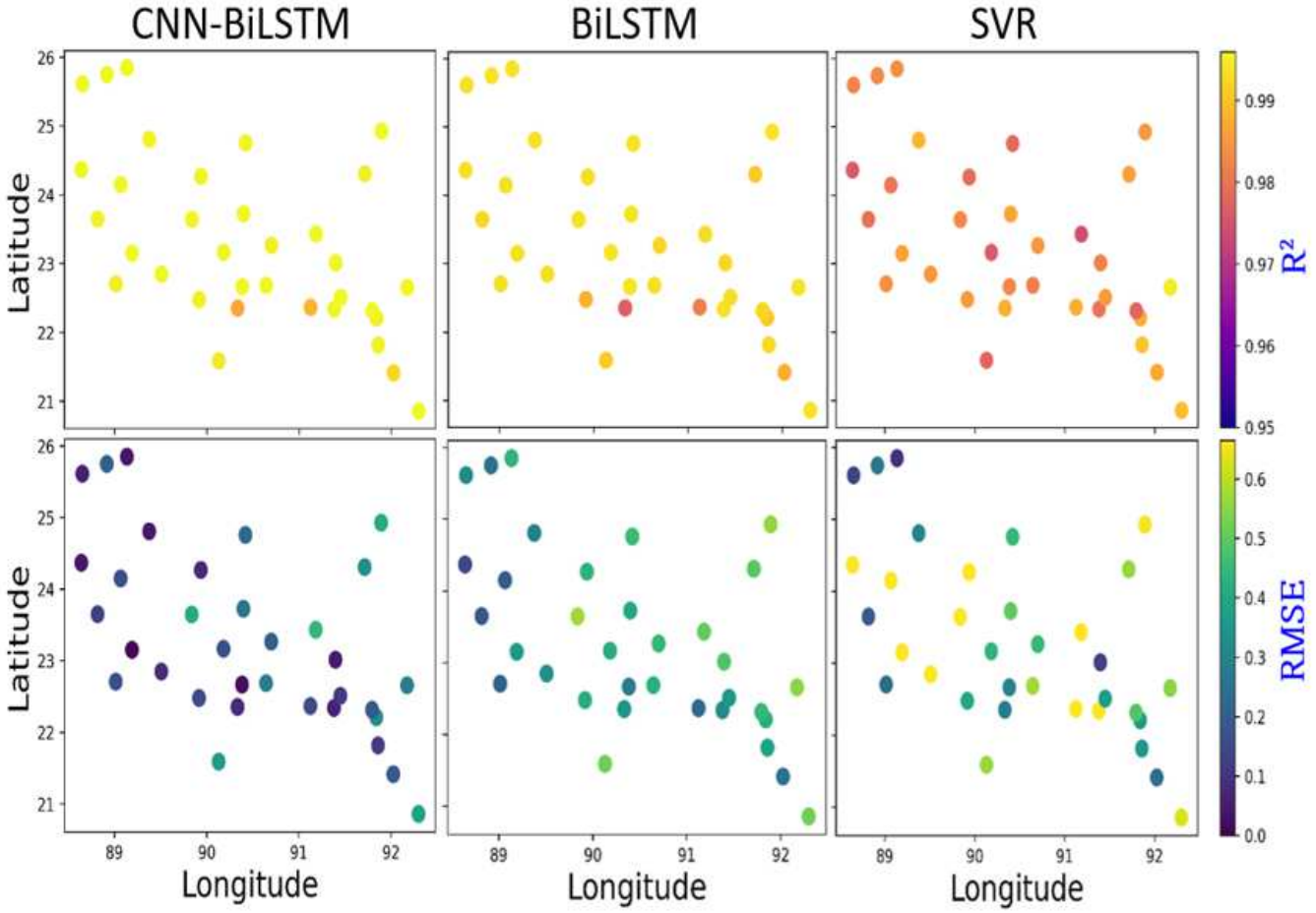

Figure 7

Geographic distribution of the coefficient of determination (R^2) and root means squared error (RMSE) acquired from the proposed hybrid model (i.e., CNN-BiLSTM) and standalone counterparts (i.e., BiLSTM and SVR) in forecasting I_F across thirty-four stations in Bangladesh.

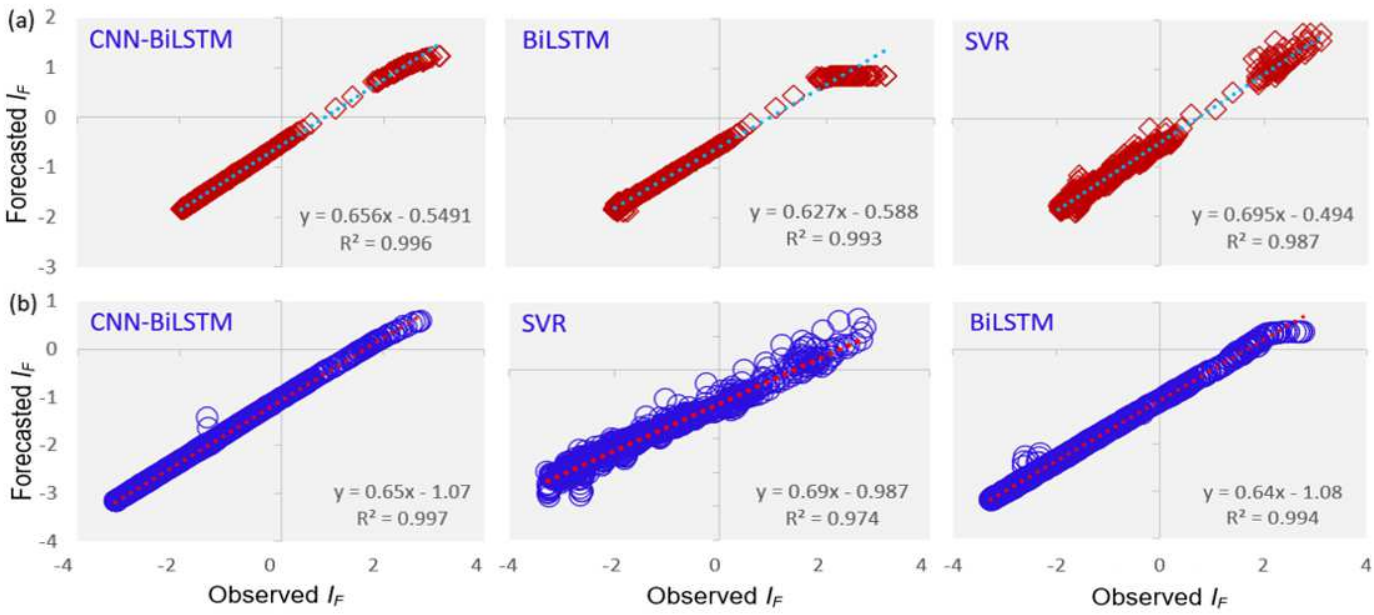

Figure 8

Scatter plot of forecasted vs. observed I_F of a) Sylhet and b) Comilla sites using the proposed hybrid model (i.e., CNN-BiLSTM) and Standalone models (i.e., BiLSTM and SVR). A least square regression line and coefficient of determination (R^2) with a linear fit equation are shown in each sub-panel.

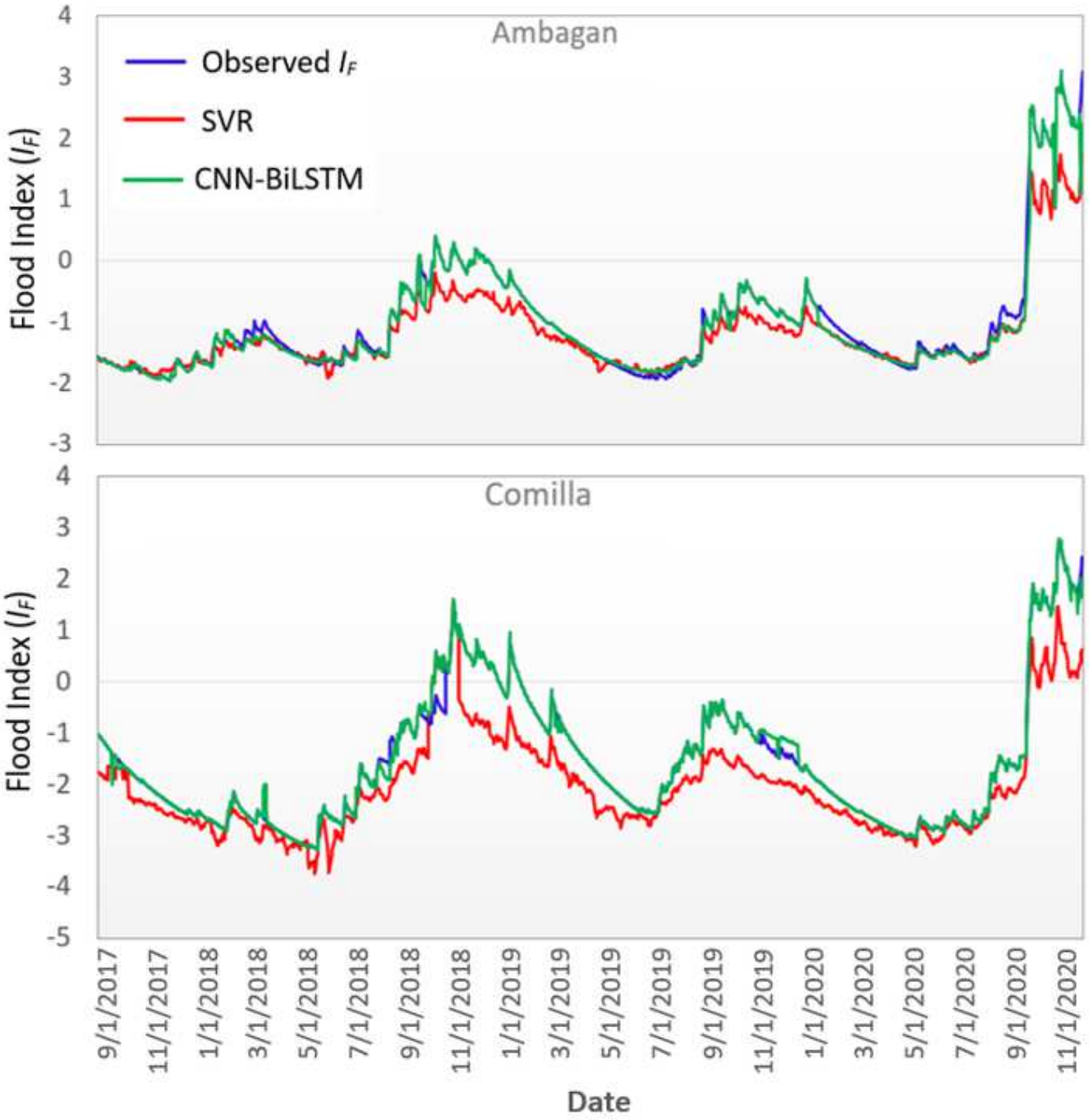

Figure 9

Comparison of time series distribution between forecasted I_F and observed I_F during model testing phase using CNN-BiLSTM vs. SVR model for Sylhet and Comilla.

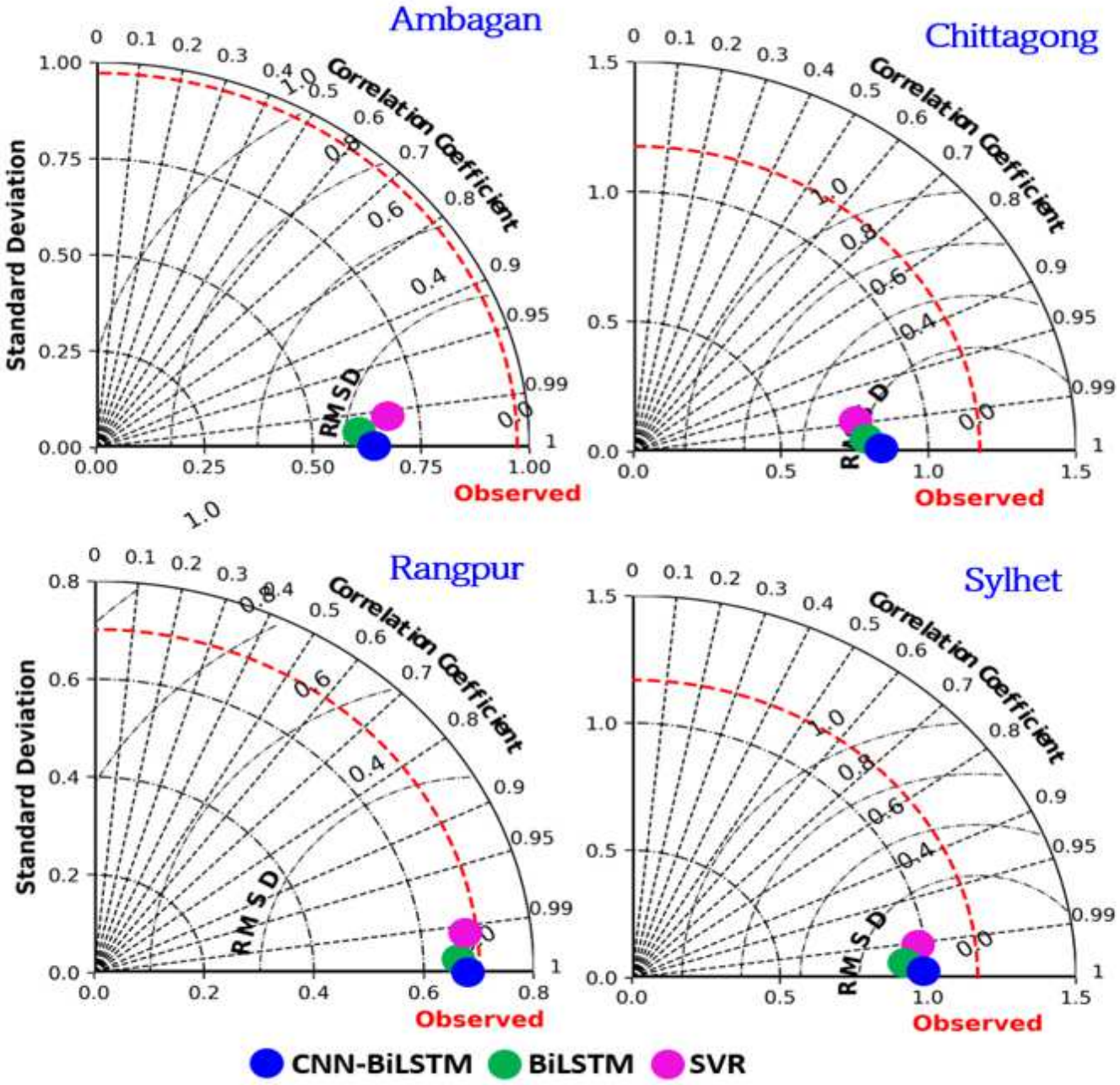

Figure 10

Tylor diagram representing correlation coefficient and the standard deviation difference for proposed hybrid CNN-BiLSTM vs. benchmark models (i.e., BiLSTM and SVR) for Ambagan, Chittagong, Rangpur, and Sylhet.

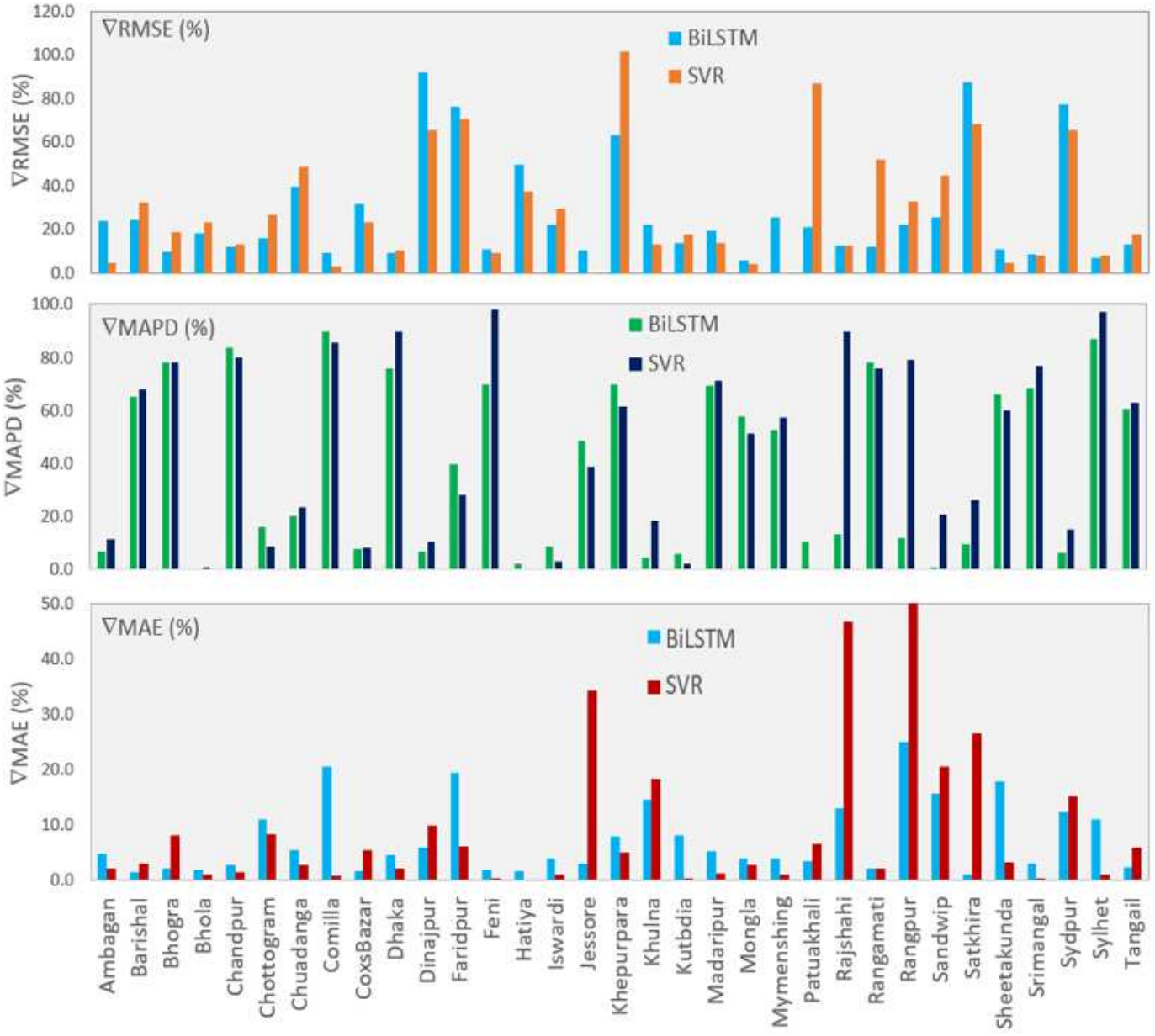

Figure 11

Promoting Percentage of RMSE (RMSE,%), MAPD (MAPD,%), and MAE (MAE, %) to illustrate the improvement percentage of the proposed model (i.e., CNN-BiLSTM) over standalone models (i.e., BiLSTM and SVR) in I_F forecasting.

Supplementary Files

This is a list of supplementary files associated with this preprint. Click to download.

- PaperFIClimateBDTabletn.docx